

Numerical study of wavelength-swept semiconductor ring lasers: the role of refractive-index nonlinearities in semiconductor optical amplifiers and implications for biomedical imaging applications

A. Bilenca, S. H. Yun, G. J. Tearney, and B. E. Bouma

Harvard Medical School and Wellman Center for Photomedicine, Massachusetts General Hospital, Boston, Massachusetts 02114

Received October 27, 2005; revised November 30, 2005; accepted December 4, 2005; posted December 8, 2005 (Doc. ID 65643)

Recent results have demonstrated unprecedented wavelength-tuning speed and repetition rate performance of semiconductor ring lasers incorporating scanning filters. However, several unique operational characteristics of these lasers have not been adequately explained, and the lack of an accurate model has hindered optimization. We numerically investigated the characteristics of these sources, using a semiconductor optical amplifier (SOA) traveling-wave Langevin model, and found good agreement with experimental measurements. In particular, we explored the role of the SOA refractive-index nonlinearities in determining the intracavity frequency-shift-broadening and the emitted power dependence on scan speed and direction. Our model predicts both continuous-wave and pulse operation and shows a universal relationship between the output power of lasers that have different cavity lengths and the filter peak frequency shift per round trip, therefore revealing the advantage of short cavities for high-speed biomedical imaging. © 2006 Optical Society of America

OCIS codes: 140.3280, 140.3600, 140.5960, 170.4500, 190.5970.

The recent development of rapidly tuning wavelength-swept lasers has enabled new high-speed biomedical imaging techniques to be developed based on optical frequency domain reflectometry^{1,2} and spectral encoding.³ To achieve fast image acquisition rates with high spatial resolution and large field of view, the imaging techniques require wavelength-swept lasers with fast repetition rates (>15 kHz), broad tuning ranges (>50 nm), and narrow instantaneous linewidths (<0.1 nm). To date, only extended-cavity semiconductor lasers that employ intracavity scanning filters have met these demanding requirements, owing to several desirable features of semiconductor optical amplifiers (SOAs) such as high small-signal gain, broadband gain spectra, and large relaxation resonance frequencies.

Perhaps the most striking observation in SOA-based ring lasers was that the sweep operation was practically limited to positive wavelength sweeps (increasing wavelength) because of the significant power loss that occurred in negative tuning.^{1,2,4,5} This asymmetric behavior was initially attributed to four-wave mixing (FWM) in SOAs causing a negative frequency shift in intracavity light as it propagates through the SOA.⁴ In this Letter we report the numerical investigation of these lasers by use of a traveling-wave Langevin model of a SOA. The calculated results reproduce the experimental observations and successfully explain the underlying physical mechanisms and their implications for biomedical imaging.

Figure 1 is a schematic of the laser in our numerical model according to the actual experimental setup previously described.⁴ It comprises a SOA as the gain medium, a linearly tuned (in time) optical filter, an

output coupler, and a fiber cavity. The numerical treatment of the SOA was based on the Langevin propagation equation^{6,7} governing the gain dynamics [g (1/m)] and the complex electric-field envelope [E (\sqrt{W})]:

$$\frac{\partial g_l(t,z)}{\partial t} = \frac{g_0 - g_l(t,z)}{\tau_s} - \frac{g(t,z)|E(t,z)|^2}{E_{\text{sat}}}, \quad (1a)$$

$$\frac{\partial E(t,z)}{\partial z} + \frac{1}{v_g} \frac{\partial E(t,z)}{\partial t} = \frac{1}{2} [g(t,z)(1 - i\alpha) - \alpha_{\text{int}}] E(t,z) + n(t,z), \quad (1b)$$

with g_l being the linear gain, g_0 the small-signal gain coefficient, τ_s the carrier lifetime, E_{sat} the saturation energy, v_g the group velocity inside the SOA, α the linewidth enhancement factor, α_{int} the waveguide losses, $\hbar\omega_0$ the single photon energy, and n_{sp} the population inversion factor. $g = g_l / (1 + \varepsilon/E^2)$ is the nonlinear gain, where ε is the nonlinear gain suppression parameter. $n(t,z)$ is a complex, spatially white, zero-mean Gaussian process representing the

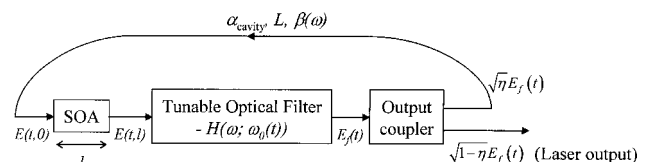


Fig. 1. Schematic diagram of the modeled wavelength-swept semiconductor ring laser incorporating a tunable (in time) intracavity filter.

spontaneous-emission noise, which has the autocorrelation function $\langle n(t, z)n^*(t', z') \rangle = \hbar\omega_0 n_{sp} g f(t-t')\delta(z-z')$, where $f(t-t') = (B/2\pi)\text{sinc}[B/2\pi(t-t')]$ and B represents the bandwidth of the optical noise spectrum. Also, $\langle n(t, z)n(t', z') \rangle = 0$. Finally, $0 \leq z \leq l$, where l is the SOA's length. To fully simulate the laser operation, Eq. (1) must be supplemented by the boundary condition

$$E(\omega, z=0) = [\eta\alpha_{\text{cavity}} H(\omega)]^{1/2} \exp[-i\beta(\omega)L]E(\omega, z=l),$$

where η is the power coupling percentage, α_{cavity} the cavity losses, $\beta(\omega)$ the propagation constant (expanded to the second-order dispersion term), and L the length of the fiber. Also, $E(\omega, z)$ denotes the Fourier transform of $E(t, z)$, and $H(\omega) = \exp\{-4 \ln 2 [\omega - \omega_0(t)]^2 / \Delta\omega^2\}$ is the Gaussian transmission function of the optical filter with ω_0 being the center frequency of the optical filter and $\Delta\omega$ its FWHM. Note that $\omega_0(t) = \text{constant}$ for a fixed filter and that $\omega_0(t)$ varies approximately linearly with time (at a constant speed, v_s) over a bandwidth of 100 nm centered at 1310 nm.

Equations (1) and the boundary condition were simulated in MATLAB by use of a split-step Fourier method. The propagation along the SOA was simulated in the time domain, whereas the boundary condition was implemented in the frequency domain. The numerical model allowed lasing to develop from the unsaturated amplified spontaneous emission of the SOA. Furthermore, the simulations equilibrated within several hundred round trips. For convenience of computational efficiency,⁸ the simulations were performed in the swept filter reference frame by use of a spectral window of 110–220 GHz and a resolution of 9–27 MHz. The window was shifted by $\Delta f_{\text{filter}} = v_s \tau_{\text{rp}}$ per round trip (τ_{rp} is the cavity round-trip time). To further confirm the results, simulations in which one round trip was divided into $m=2, 4, 8, 16$ sections and $\Delta f_{\text{filter}} = v_s \tau_{\text{rp}} / m$ were also executed. A net small-signal gain of 29 dB and n_{sp} of 4.7 (both deduced from measurements) as well as representative SOA values, i.e., $\tau_s = 380$ ps, $\varepsilon = 0.7 \text{ W}^{-1}$, $E_{\text{sat}} = 3.8$ pJ, $v_g = 8.427 \times 10^7$ m/s, and $\alpha = 5$, were used throughout the calculations. Also, unless otherwise stated, $\hbar\omega_0 = 1.517 \times 10^{-19}$ J, $\eta = 0.11$, $\alpha_{\text{cavity}} = 0.4$, $\beta_2 = 1 \text{ ps}^2/\text{km}$, $L = 7.4$ m, and $\Delta\omega = 2\pi(21 \times 10^9 \text{ rad/s})$.

First we computed the normalized power spectrum of the intracavity field emerging from the SOA output and of the cw laser output field under fixed optical filtering conditions [i.e., $\omega_0(t) = 2\pi c/1310 \text{ nm}$] along with the transmission spectrum of the filter, as shown in Fig. 2(a) by solid, dashed, and dashed-dotted curves, respectively. These computations were performed with $\eta = 0.9$ and $\alpha_{\text{cavity}} = 0.36$, and good correspondence with measured optical spectra (at a resolution bandwidth of 0.1 nm) was obtained, as shown in Fig. 2(b). It can be clearly observed that the SOA shifts the input spectrum toward lower frequencies. Moreover, we note that the field spectrum at the SOA output is asymmetrically broadened. These spectral effects are caused by the SOA nonlinearities, primarily carrier-induced refractive-index changes,

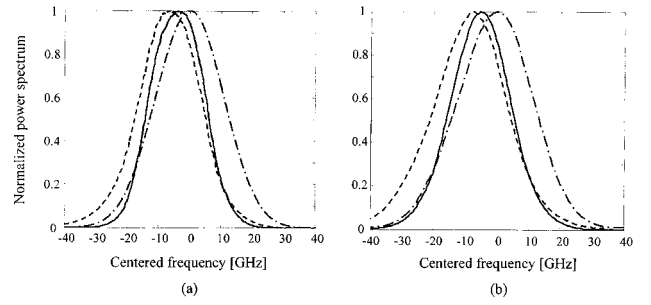


Fig. 2. Spectral characteristics of the laser for a fixed filter wavelength: (a) simulated results, (b) experimental data. Solid curves, laser output; dashed curves, SOA output; dashed-dotted curves, filter function.

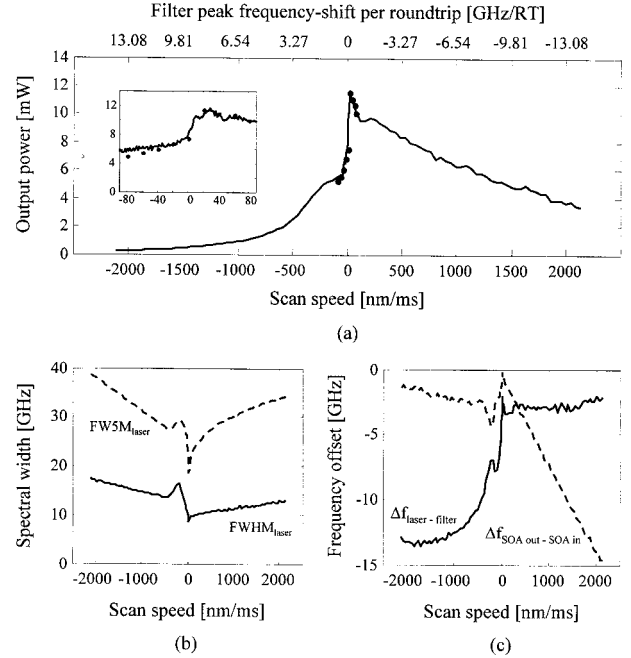


Fig. 3. Laser characteristics versus scanning speed: (a) output power, (b) spectral width, (c) frequency offset.

which are responsible for self-phase modulation⁹ (SPM) and asymmetric FWM among different spectral components of the broadband field.¹⁰ The latter is related to the so-called Bogatov effect¹¹ and is responsible for the spectrum asymmetry (SPM alone would have generated a symmetric quasi-cw spectrum⁹). Furthermore, the frequency shift and spectral broadening introduced by the SOA are reduced as the α parameter decreases and nearly vanish at $\alpha = 0$.

Next, we simulated the laser output power as a function of filter scan speed, as described in Fig. 3(a). The corresponding values of the filter peak frequency shift per round trip are also shown. The theoretical curve demonstrates good correspondence with experimental data from Ref. 4, which are represented as discrete points. Figure 3(a) highlights interesting features of the wavelength-swept SOA ring laser: The maximum output power is obtained at a low, positive scanning speed, and the drop in power away from this maximum is asymmetric. The low power observed at negative speeds (decreasing wavelength) is readily understood, considering that the filter wave-

length offset on each round trip is opposite in sign from the nonlinear redshift that arises during transmission through the SOA. As the filter speed is increased toward positive values, filter loss diminishes and intracavity power increases and saturates the SOA. Hence the magnitude of the SOA-induced frequency shift decreases⁹ until it becomes matched to the filter offset per round trip as described in Fig. 3(c) by the dashed curve, which represents the offset between the peaks of the SOA output and input spectra ($\Delta f_{\text{SOAout-SOAin}}$). This resonant matching effect⁸ reduces the laser linewidth [Fig. 3(b): solid curve, FWHM; dashed curve (FW5M), full width at 5% of the maximum amplitude) as well as the magnitude of the offset between the lasing peak spectrum and the center frequency of the optical filter [i.e., $\Delta f_{\text{laser-filter}}$ in Fig. 3(c), solid curve). Further increasing the filter scanning speed reduces the SOA saturation level such that larger frequency shifts can be mediated by the amplifier [i.e., $\Delta f_{\text{SOAout-SOAin}}$ increases, as one can observe from Fig. 3(c)].⁹ Then the SOA output spectrum can successfully follow the scanned filter spectrum, thus resulting in a value of $\Delta f_{\text{laser-filter}}$ that is approximately constant, as illustrated in Fig. 3(c). Essentially, the SOA gain nonlinearities assist in preserving the resonant operation of the laser; however, this comes at the expense of a lower emitted power [Fig. 3(a)] and a broader lasing linewidth [Fig. 3(b)]. Our model reveals that the dependence of the output power from lasers that have different cavity lengths on the filter's peak frequency shift per round trip is *universal* and follows the curve shown in Fig. 3(a). This behavior is expected because the operation of the wavelength-swept ring lasers is governed by the interplay between the frequency shift and the change in the filter's peak position per round trip.⁸ This re-

sult implies that improved performance of high tuning speed lasers will result from decreased cavity lengths, as indicated also in Ref. 2. It is worth mentioning that, for negative values of the filter's frequency shift per round trip with magnitude comparable with or larger than the reciprocal of the interband carrier relaxation time, these calculations yielded quasi-periodic pulsation rather than cw operation, as shown in Fig. 4(a). The self-pulsation operation is presumably due to the balance between frequency shifting and spectral broadening through SOA nonlinearities, and subsequent spectrum trapping by the swept filter. Note that in contrast to the cw operation regime, for which both SPM and FWM contribute to the spectral intracavity field characteristics, here the formation of pulses suggests that the large SOA-induced frequency shifts are due mainly to SPM.⁹ This conclusion is additionally supported by the multipeak spectrum structure observed in this operation regime. Finally, Fig. 4(b) describes the *normalized* output power relative to the center filter frequency shift per round trip for several values of the α parameter. Larger α parameter values assist resonant operation with higher output power at large negative-frequency-direction scanning speeds by matching the swept filter and lasing frequency shifts per round trip, as identified by the inset of Fig. 4(b).

In conclusion, our simulation results for wavelength-swept SOA ring lasers suggest that a short cavity length and a large α parameter will improve the *unidirectional* sweeping power characteristics, whereas a short cavity length and a small α parameter (with quantum dot-dash gain material) will improve the *bidirectional* sweeping performance. Finally, further investigations of the self-pulsation operation in these sources are merited.

The authors gratefully acknowledge funding support from Terumo Corporation. A. Bilenca's e-mail address is abilenca@partners.org.

References

1. S. H. Yun, G. J. Tearney, J. F. de Boer, N. Iftimia, and B. E. Bouma, *Opt. Express* **11**, 2953 (2003).
2. R. Huber, M. Wojtkowski, K. Taira, J. G. Fujimoto, and K. Hsu, *Opt. Express* **13**, 3513 (2005).
3. C. Boudoux, S. H. Yun, W. Y. Oh, W. M. White, N. V. Iftimia, M. Shishkov, B. E. Bouma, and G. J. Tearney, *Opt. Express* **13**, 8214 (2005).
4. S. H. Yun, C. Boudoux, M. C. Boudoux, J. F. de Boer, G. J. Tearney, and B. E. Bouma, *IEEE Photonics Technol. Lett.* **16**, 293 (2004).
5. M. A. Choma, K. Hsu, and J. A. Izatt, *J. Biomed. Opt.* **10**, 044009 (2005).
6. M. Shtaif and G. Eisenstein, *IEEE J. Quantum Electron.* **32**, 1801 (1996).
7. A. Mecozzi and J. Mørk, *IEEE J. Sel. Top. Quantum Electron.* **3**, 1190 (1997).
8. S. H. Yun, D. J. Richardson, D. O. Culverhouse, and B. Y. Kim, *IEEE J. Sel. Top. Quantum Electron.* **3**, 1087 (1997).
9. G. P. Agrawal and N. A. Olsson, *IEEE J. Quantum Electron.* **25**, 2297 (1989).
10. G. P. Agrawal, *J. Opt. Soc. Am. B* **5**, 147 (1988).
11. A. P. Bogatov, P. G. Eliseev, and B. N. Sverdlov, *IEEE J. Quantum Electron.* **11**, 510 (1975).

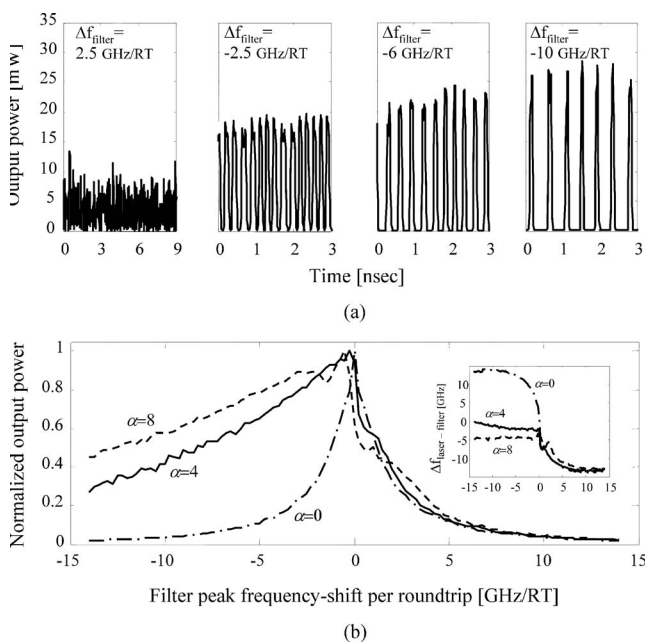


Fig. 4. (a) Temporal power signals at the laser output calculated for four values of filter peak frequency shift per round trip (RT), (b) normalized output power computed for three α parameter values. Inset, corresponding laser-filter frequency offset values.